Eur. Phys. J. Plus (2017) **132**: 481
DOI 10.1140/epjp/i2017-11749-4

THE EUROPEAN PHYSICAL JOURNAL PLUS

Regular Article

Analysis of size-dependent smart flexoelectric nanobeams

Rahim Omidian[1], Yaghoub Tadi Beni[2,a], and Fahimeh Mehralian[1]

[1] Department of Mechanical Engineering, Shahrekord University, Shahrekord, Iran
[2] Faculty of Engineering, Shahrekord University, Shahrekord, Iran

Received: 21 April 2017 / Revised: 8 September 2017
Published online: 21 November 2017 –

Abstract. In this paper, the flexoelectric formulations of Timoshenko nanobeams are developed and the static deflection as well as the free vibration of nanobeams are extracted from the formulation under direct and inverse flexoelectric effects. Considering both the direct and the inverse flexoelectric effects, the governing equations and the associated boundary conditions of the nanobeams are developed. Afterwards, static and vibrational analyses are conducted on the Timoshenko and Euler-Bernoulli nanobeams subjected to cantilever and simply supported boundary conditions. Also, the exact solutions for the displacements and the electric potential are obtained in the static analysis. Finally, the effects of the flexoelectric coefficient and the size effect parameter on natural frequency, nanobeam deflection and electric field are investigated. The formulation developed in this study is validated by drawing a comparison between the present results and the results of previous studies. The results presented in this work might help to design advanced smart nanostructures in future studies.

1 Introduction

Beams play a significant role in mechanical and electromechanical systems, such as sensors and actuators. They are often subjected to dynamic and static excitation. As the issue of vibration and natural frequency has been a significant subject in beam analysis, many studies have been conducted on the natural frequency and the form of elastic beam modes.

Today, micro/nanosystems occupy an indispensable position in many scientific and industrial areas. The function of many of these systems is based upon the deformation of a beam in micro/nanodimensions; hence, it is especially important to study and control the behavior of micro/nanobeams. Among micro/nanobeams, cantilever and clamped-clamped beams, which are actuated through electrostatic or piezoelectric excitation, enjoy more extensive application. Cantilever beams, for instance, are used in atomic force microscopy, microswitches, and accelerometers, and clamped-clamped beams are used in micromirrors and light regulation windows.

Smart materials continue to have increasing application in controlling vibration in different structural parts of airplanes, satellites, satellite carriers, submarines, automobiles, helicopter blades, and other highly sensitive systems. In aerospace structures, in particular, due to weight and size limitation, it is very difficult to control vibration through common methods. The emergence of new technologies (*i.e.* smart materials) in engineering, in the last two decades, has paved the way for the investigation of active dissipation of structural vibration. In this connection, due to their low weight, acceptable energy consumption, and precise handling capability, piezoelectric technologies have been extensively used in accurate and active vibration control in structures.

The flexoelectric effect might be identified through the piezoelectric effect. Piezoelectric materials have a non-centrosymmetric property, which is present only in 20–32 crystal structures with specific symmetry classification, whereas such a limitation is not posed by the flexoelectric effect, in which materials with any sort of symmetry are capable of triggering electromechanical coupling. In electromechanical coupling, the bending of one crystal leads to the pulling of its atomic layers, whereby the outermost layer receives the greatest pulling force. This variation of the pulling force in different layers can displace ions in the crystal so frequently that an electric field is created. In fact, a non-homogeneous strain gradient or strain field can create polarization in dielectric materials with central symmetry due to local faults, a phenomenon referred to as (direct) flexoelectric effect. The flexoelectric effect generally refers

[a] e-mail: tadi@eng.sku.ac.ir (corresponding author)

to the coupling created within electric polarization caused by strain gradient (direct flexoelectric) or to elastic stress caused by polarization gradient (inverse flexoelectric) [1,2].

Generally, in contrast to the piezoelectric effect, the flexoelectric effect is a rare phenomenon. Nonetheless, the flexoelectric effect can rival, and sometimes defeat, the piezoelectric effect in the nanoscale, since the gradient is higher in smaller dimensions. Furthermore, due to a lack of symmetry in the flexoelectric effect, a broader range of materials can be used as electromechanical sensors [3,4].

In recent years, mechanical and electric properties of flexoelectric and piezoelectric materials have been investigated using experimental methods and precise measurement instruments. Studies have demonstrated that the mechanical and electric properties of piezoelectric and flexoelectric materials in the nanoscale hold a relationship with the size effect [5–8]. Moreover, using the size-dependent theories, researchers have investigated the formulation of flexoelectric and piezoelectric beams and extracted their mechanical and electric properties [9,10]. In one study, Yan and Jiang examined the flexoelectric effect on the mechanical and electric properties of Timoshenko [11] and Euler-Bernoulli [12] beams using the theory put forth by Hu and Shen [13]. Tadi [14] investigated piezoelectric nanobeams by taking the flexoelectric effect into consideration. He developed the nonlinear formulation of the Timoshenko beam using the size-dependent piezoelectric theory and developed the governing equations and boundary condition using Hamilton's principle. Finally, he compared the free vibration and static deflection results with the results of the classical theory for a hinged-hinged beam. In another study, Tadi [15] developed the nonlinear formulation of Euler-Bernoulli beams with isotropic piezoelectric materials using the size-dependent piezoelectric theory and compared the results of hinged-hinged static and vibrational nanobeam with the results of the classical linear and nonlinear theory. Many researchers have investigated size effects on flexoelectric and piezoelectric materials using the flexoelectric theory. Li *et al.* [16] examined three-layer Euler-Bernoulli microbeams subjected the flexoelectric effect using Hajesfandiari's [17] piezoelectric theory and obtained results regarding size-dependent vibration and bending. Liang and Shen [18], in accordance with the theory developed by Hu and Shen [13], investigated piezoelectric nanowires using the size-dependent Euler-Bernoulli beam model.

Since the identification of the equations governing micro/nanoscale system plays a significant role in predicting their behavior and the effects of different parameters on their functioning, and because such knowledge is necessary for optimal design of such systems, it is imperative to use models which predict the behavior of such system with maximum precision and minimum errors and costs. To this end, theories based upon continuum mechanics are currently utilized. Higher-order continuum theories currently used in nanostructure modeling include the non-local theories, coupe stress theory, and strain gradient theory. These theories yield more appropriate solutions in comparison to classical theories by incorporating extra parameters into modeling size effects. Zhao *et al.* [19] used Hamilton's principle and strain gradient theory to find the nonlinear governing equations of microbeams. In another study, Sadeghi *et al.* [20] used the strain gradient theory to demonstrate the effect of the small scale on the bending, vibration, and stability of functionally graded (FG) microbeams. Ke *et al.* [21] determined the natural frequency and the mode shapes of piezoelectric nanobeams using the non-local elasticity theory. They used the linear model to investigate the effects of temperature variation, voltage, axial load, and the size coefficient on natural frequency and mode shapes, demonstrating the significance of incorporation of size effects.

In the light of the foregoing discussion, use of higher-order continuum theories to demonstrate the flexoelectric effect requires modification of the expression of the theories. To this end, Li *et al.* [1] recently developed a new theory based upon the strain gradient theory for the flexoelectric effect, which models size effects as well. The present paper uses this new theory.

The extensive application of micro/nanobeams has encouraged many researchers to study their static and dynamic behavior through various methods. Determining the static displacement and vibration plays a remarkable role in the design process of nanoscale systems. Studying the vibrational behavior of such systems is effective in selecting the parameters for designing actuators and sensors. Generally, the vibration characteristic of these beams is investigated with the assumption of minute vibration around a deformed state. Huang *et al.* [22] conducted a static analysis on a microbeam actuated by electric field. They computed the Taylor series to the third order for the electric force applied to the microbeam, analytically determining the static displacement and tensile instability voltage for clamped-clamped and cantilever boundary conditions by using Galerkin method and by taking one mode into consideration (it is worth mentioning that the extension of the middle plane is taken into account for clamped-clamped boundary conditions). Afterwards, they compared their results with the numerical Garlekin – Newton-Raphson results. Their results differed from the numerical results only with respect to tensile instability, which was mainly due to the extension of the electric force in the static equation. By computing the derivative of the energy equation and by taking one mode into consideration, Ho [13] analytically determined the displacement of a curved microbeam actuated by an electric field and computed its tensile instability voltage. Zamanian *et al.* [23] conducted a static and dynamic analysis of a unimorph microbeam subjected to electrostatic and piezoelectric excitation by taking into consideration the nonlinear effects of the mid-layer tension. They computed the effect of length and thickness of the piezoelectric layer, direct piezoelectric voltage, and direct electrostatic voltage on the natural frequency, static deflection, and pull-in voltage. Li *et al.* [24] investigated the free vibration of an FG material with piezoelectric layers subjected to temperature and

voltage. They determined the beam motion equations under electric and thermal loading conditions by taking into consideration the precise degree of longitudinal tension based upon the classical beam theory. Ghayesh *et al.* [25] investigated the forced nonlinear vibration of a microbeam, using the strain gradient elasticity theory to examine the small scale effects.

The majority of studies conducted on axially moving beams have used Euller-Bernoulli beams, in which the effects of transverse shear deformation and rotational inertia are ignored, resulting in significant error in cases where the cross-section dimensions are not small in comparison to length. Despite the considerable body of research on axially moving beams, few studies have used the Timoshenko beam theory, which is free from the disadvantages of the Euler-Bernoulli beam model and the results of which are acceptable and sufficiently accurate from low to high length–to–cross-section ratios. The equations of axially moving Timoshenko beams were first developed by Simpson [26], and the vibration behavior of Timoshenko beams has been investigated by various researchers. By way of example, Davis and Henshell [27] investigated the effect of shear coefficient on natural frequencies of beams and examined the results for simply supported and clamped beams. Thomas *et al.* [28], Kapur [29], and Tabarrok and Cleghorn [30] developed various mathematical models for investigating the vibration of Timoshenko beams. Zhang *et al.* [31] investigated the static bending, free vibration, and buckling of microbeams using the Timoshenko beam theory and strain gradient elasticity theory. Ke *et al.* [21] studied the free vibration and elastic buckling of a targeted cracked beam based on the Timoshenko beam theory through the analytical method. Also, Şimşek [32] conducted a nonlinear vibration analysis of an FG Timoshenko beam subjected to moving load with harmonic excitation and drew a comparison between the results of nonlinear analysis based on Timoshenko theory and those based on the classical theory. However, in recent years the modeling of variety of nanostructures have been examined which have different materials and different applications [33–42].

The computational methods for solving the smart flexoelectric/ piezoelectric nanobeams is also important issue that must be considered. In recent years, a large number of methods were developed to find the solutions for the governing equation of nanobeams which are linear and nonlinear partial differential equations. For example, recently Yang *et al.* [43–45] used exact traveling-wave solution for the analysis of some local fractal equations. However, in this paper the exact solution is obtained for the displacements and the electric potential.

Great achievements have been made in smart structures through using a flexoelectric materials. Due to a lack of symmetry in the flexoelectric effect, a broader range of materials can be used as electromechanical sensors. Also these superiorities attracted the attention of a lot of researchers toward felexoelectric materials in different structural elements and engineering applications such as sensors and actuators. Accordingly, the comprehensive understanding of their behavior is therefore a major area of research for reliable design of smart structures. However, the difficulty and complexity of examination of flexoelectric structures leads to only a few investigations in the open literature.

On the other hand, nanobeams are found to be principle elements in most nanoelectromechanical systems. Besides, nanoelectromechanical systems are extensively used in different dynamic, thermal, chemical, optic, magnetic, electrical fields. Moreover, due to the difficulties of nanoscale experiments and time consuming of atomistic simulation, the higher-order continuum theories, as efficient alternative approaches, have been developed to analyze the bending, buckling and vibration of nanostructures. Motivated by these considerations, this paper for the first time investigates the static deflection and vibration behavior of felexoelectric nanobeams based on the flexoelectric theory proposed by Li *et al.* [1]. The formulation is developed on the basis of Timoshenko beam model. The governing equations and boundary conditions are derived using the Hamilton's principle. The novelty of the formulation derived herein is that it benefits from the following characteristics simultaneously:

- First, this formulation is utilized for studying static and dynamic behaviors of felexoelectric materials.
- Second, this formulation is able to predict the behavior of beam structures more realistically due to using the Timoshenko beam model.
- Third, the size effect is considered in this formulation and this formulation can be reduced into the classical beam formulation as well.
- Fourth, the shear deformation theory enables this formulation to be utilized for shorter and thicker beams.
- Fifth, the exact solutions for the displacements and the electric potential is obtained in this analysis.

Also, as a case study, the static bending and vibration behaviors of cantilever and simply supported, nanobeams, are investigated. The effects of flexoelectric coefficient and size effect parameter on natural frequency, nanobeam deflection, and electric field are investigated.

The structure of the present paper is as follows: First, the formulation of flexoelectric materials is briefly outlined, the flexoelectric theory for isotropic dielectric materials is introduced, and equations of motion and boundary conditions for Timoshenko beam model are extracted. Afterwards, the results of static deformation of beams subjected to direct and inverse flexoelectric effect are investigated, extracted, and analyzed for the two Timoshenko and Euler-Bernoulli models, and the free vibration of the beams are examined. Finally, the governing equations are solved, the results are analyzed, and the effects of various parameters on the results are investigated.

2 Preliminary

According to the theory developed for dielectric materials [13,46], the most general description for internal energy density (U) is formulated in such a way that internal energy density is dependent not only upon strain and polarization, but also upon their gradients. Therefore, one can write

$$U = U\left(\varepsilon_{ij}, \eta_{ijk}, P_i, Q_{ij}\right), \tag{1}$$

where ε_{ij} denotes strain tensor components, $\eta_{ijk} = \varepsilon_{jk,i}$ denotes strain gradient components, P_i represents polarization vector components, and $Q_{ij} = P_{i,j}$ stands for polarization gradient components. The strain tensor is defined as

$$\varepsilon_{ij} = \frac{1}{2}(u_{i,j} + u_{j.i}), \tag{2}$$

where u_i represents displacement vector components. According to the equations extracted by Hu *et al.* [47], the structural equations based on internal energy density are

$$\sigma_{ij} = \frac{\partial U}{\partial \varepsilon_{ij}}, \quad \tau_{ijk} = \frac{\partial U}{\partial \eta_{ijk}}, \quad E_i = \frac{\partial U}{\partial P_i}, \quad V_{ij} = \frac{\partial U}{\partial Q_{ij}}, \tag{3}$$

where σ_{ij} represent stress tensor components, E_i stands for electric field components, and τ_{ijk} and V_{ij} are higher-order stress and electric field components, respectively. Hence, using eq. (3), the internal energy density equation is given by

$$U = \frac{1}{2}\sigma_{ij}\varepsilon_{ij} + \frac{1}{2}\tau_{ijk}\eta_{ijk} + \frac{1}{2}E_iP_i + \frac{1}{2}V_{ij}Q_{ij}. \tag{4}$$

Using the equation introduced by Toupin [8], electric enthalpy density is expressed in such a way that it includes flexoelectricity as

$$H = U - \frac{1}{2}\varepsilon_0\varphi_{,i}\varphi_{,i} + \varphi_{,i}P_i, \tag{5}$$

where ε_0 represents vacuum permittivity, and φ is Maxwell potential, which is defined as follows:

$$E_i^{MS} = -\varphi_{,i}. \tag{6}$$

Therefore, using the Raynolds transport theorem, the total electric enthalpy variation of a flexoelectric structure is given by [48]

$$\delta \int_V H \mathrm{d}V = \int_V \delta H \mathrm{d}V + \int_V H\delta u_{k,k} \mathrm{d}V \tag{7}$$

and the kinetic energy of the beam is defined as

$$K = \int_v \frac{1}{2}\rho\left[\dot{u}_1^2 + \dot{u}_2^2 + \dot{u}_3^2\right] \mathrm{d}V, \tag{8}$$

where ρ is the density of the material used.

Considering the application of the extensive force $q(x)$ as well as the concentrated shear force $\overline{V}$ and the axial force $\overline{N}$ the equation of virtual work done by external loads is written as

$$\delta W = \int_v q(x,t)\delta w \mathrm{d}V + \left(\overline{N}\delta u_0\right)\Big|_{x=0}^{x=L} + \left(\overline{V}\delta w\right)\Big|_{x=0}^{x=L}. \tag{9}$$

Finally, Hamilton's principle can be used to extract the governing equations as

$$\delta \int_0^T \left(-H + K + W\right) \mathrm{d}t = 0. \tag{10}$$

3 Flexoelectric theory for isotropic dielectric materials

This study uses the theory developed by Li *et al.* [1], which defines the strain energy density relationship as follows:

$$U = \frac{1}{2}\sigma_{ij}\varepsilon_{ij} + \frac{1}{2}p_i\gamma_i + \frac{1}{2}\tau^{(1)}_{ijk}\eta^{(1)}_{ijk} + \frac{1}{2}m'_{ij}\chi'_{ij} + \frac{1}{2}E_iP_i + \frac{1}{2}V_{ij}Q_{ij}, \tag{11}$$

where

$$\begin{aligned}
\sigma_{ij} &= \frac{\partial U}{\partial \varepsilon_{ij}} = k\delta_{ij}\varepsilon_{nn} + 2\mu\varepsilon'_{ij} - f_1\delta_{ij}Q_{kk} - 2f_2Q_{ij},\\
p_i &= \frac{\partial U}{\partial \gamma_i} = 2\mu l_0^2\gamma_i + \left(f_1 + \frac{2}{3}f_2\right)P_i,\\
\tau^{(1)}_{ijk} &= \frac{\partial U}{\partial \eta^{(1)}_{ijk}} = 2\mu l_1^2\eta^{(1)}_{ijk},\\
m'_{ij} &= \frac{\partial U}{\partial x'_{ij}} = 2\mu\left(l_2^2 + \frac{9}{5}l_0^2\right)x'_{ij} + 2\mu\left(l_2^2 - \frac{9}{5}l_0^2\right)x'_{ji} + 2f_2e_{ijk}P_k,\\
E_i &= \frac{\partial U}{\partial P_i} = \alpha P_i + \left(f_1 + \frac{2}{3}f_2\right)\gamma_i + 2f_2e_{ijk}\chi'_{jk},\\
V_{ij} &= \frac{\partial U}{\partial Q_{ij}} = \alpha\left(\delta_{ij}\beta_1^2Q_{nn} + \beta_2^2Q_{ij} + \beta_3^2Q_{ji}\right) - f_1\delta_{ij}\varepsilon_{nn} - 2f_2\varepsilon_{ij},
\end{aligned} \tag{12}$$

where the moduli λ and μ have the same meaning as Lamé constants for an isotropic material in Cauchy elasticity; l_i ($i = 1, 2, 3$) and β_i ($i = 1, 2, 3$) are length scale parameters with the dimension of length associated with the strain gradient and polarization gradient, respectively; also, δ denotes the Knocker delta, $\tau^{(1)}_{ijk}$, p_i, m'_{ij} are the higher-order stresses, and f, α are the flexoelectric coefficient and reciprocal dielectric susceptibility, respectively.

The components of the strain tensor, the dilatation gradient tensor, the deviatoric stretch gradient tensor, and the deviatoric curvature tensor are represented by ε_i, γ_i, $\eta^{(1)}_{ijk}$, χ'_{ij}, respectively, and are defined as

$$\begin{aligned}
\chi'_{ij} &= e_{ipq}\varepsilon'_{jq,p},\\
\gamma_i &= \varepsilon_{mm,i},\\
\varepsilon_{kj,i} &= \varepsilon'_{kj,i} + \frac{1}{3}\delta_{jk}\varepsilon_{nn,i},\\
\eta^{(1)}_{ijk} &= \frac{1}{3}\left(\varepsilon_{jk,i} + \varepsilon_{ki,j} + \varepsilon_{ij,k}\right) - \frac{1}{15}\delta_{ij}\left(\varepsilon_{mm,k} + 2\varepsilon_{mk,m}\right) - \frac{1}{15}\left[\delta_{jk}\left(\varepsilon_{mm,i} + 2\varepsilon_{mi,m}\right) + \delta_{ki}\left(\varepsilon_{mm,j} + 2\varepsilon_{mj,m}\right)\right].
\end{aligned} \tag{13}$$

4 Governing equations of motion and related boundary conditions

In investigating nanobeams, the first the beam is modeled using the Timoshenko model. Afterwards, equations of motion and boundary condition are developed using the non-classical flexoelectric theory and Hamilton's principle. The electric field is considered only along beam thickness [49]. Therefore, the equations and boundary conditions are determined by considering the non-zero elements of electric field along the z-direction. Finally, the equations of motion and boundary conditions determined for the flexoelectric beam.

Figure 1 illustrates the schematic representation of a Timoshenko beam. According to this illustration, the coordinate system is considered to be positioned on the middle plane of the beam, such that x is along the direction of the beam length and z is perpendicular to it. L represents beam length and h stands for beam thickness.

The displacement field of the beam based on the Timoshenko beam model is considered to be [27]

$$\begin{aligned}
u(x, z, t) &= u_0(x, t) - z\psi(x, t)\\
v &= 0,\\
w &= w(x, t),
\end{aligned} \tag{14}$$

where u_0 and w represent the displacements along the x- and z-axis of the middle surface, respectively, and ψ stands for beam cross-section rotation. By substituting eq. (14) into eq. (2), the non-zero components of strain are determined

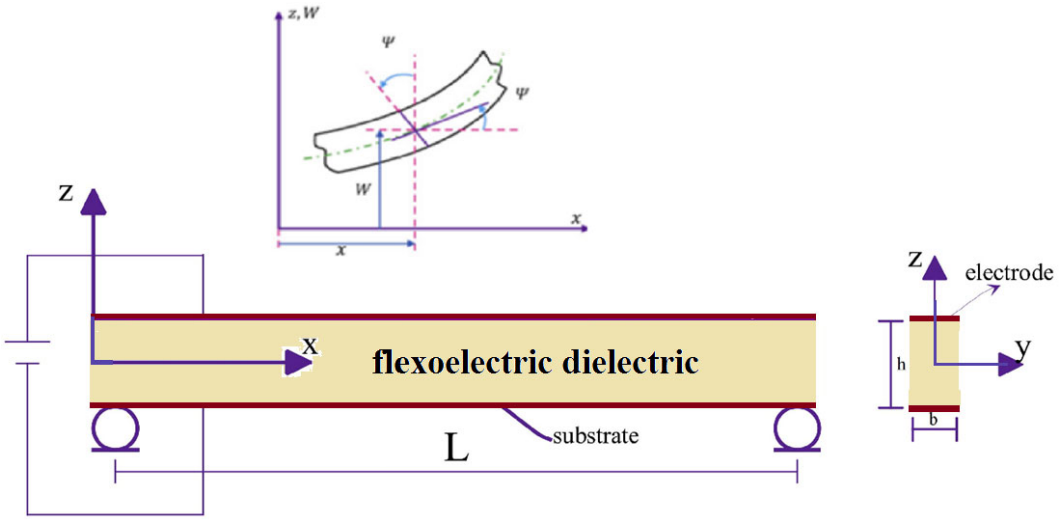

Fig. 1. Timoshenko beam model, kinematic parameters, coordinates, and geometry of the system.

as

$$\varepsilon_{11} = \frac{\partial u_1}{\partial x} = \frac{\partial u_0}{\partial x} - z\frac{\partial \psi}{\partial x}\,,$$
$$\varepsilon_{13} = \frac{1}{2}\left(\frac{\partial w}{\partial x} - \psi\right). \tag{15}$$

By substituting eq. (15) into eq. (13), the non-zero components are extracted as

$$\chi'_{12} = -\frac{1}{3}\frac{\partial \psi}{\partial x}\,,$$
$$\chi'_{21} = -\frac{1}{6}\frac{\partial \psi}{\partial x} - \frac{1}{2}\frac{\partial^2 w}{\partial x^2}\,,$$
$$\chi'_{23} = \frac{1}{3}\left(\frac{\partial^2 u_0}{\partial x^2} - z\frac{\partial^2 \psi}{\partial x^2}\right),$$
$$\chi'_{32} = -\frac{1}{3}\left(\frac{\partial^2 u_0}{\partial x^2} - z\frac{\partial^2 \psi}{\partial x^2}\right), \tag{16}$$
$$\gamma_1 = \frac{\partial^2 u_0}{\partial x^2} - z\frac{\partial^2 \psi}{\partial x^2}\,,$$
$$\gamma_3 = -\frac{\partial \psi}{\partial x}\,, \tag{17}$$
$$\eta^{(1)}_{111} = \frac{2}{5}\left(\frac{\partial^2 u_o}{\partial x^2} - z\frac{\partial^2 \psi}{\partial x^2}\right),$$
$$\eta^{(1)}_{313} = \eta^{(1)}_{331} = \eta^{(1)}_{133} = \frac{-1}{5}\frac{\partial^2 u_o}{\partial x^2} + \frac{1}{5}z\frac{\partial^2 \psi}{\partial x^2} = \eta^{(1)}_{221} = \eta^{(1)}_{122} = \eta^{(1)}_{212},$$
$$\eta^{(1)}_{333} = -\frac{1}{5}\left(\frac{\partial^2 w}{\partial x^2} - 2\frac{\partial \psi}{\partial x}\right),$$
$$\eta^{(1)}_{113} = \eta^{(1)}_{131} = \eta^{(1)}_{311} = \frac{4}{15}\left(\frac{\partial^2 w}{\partial x^2} - 2\frac{\partial \psi}{\partial x}\right),$$
$$\eta^{(1)}_{223} = \eta^{(1)}_{232} = \eta^{(1)}_{322} = -\frac{1}{15}\left(\frac{\partial^2 w}{\partial x^2} - 2\frac{\partial \psi}{\partial x}\right). \tag{18}$$

Given that the electric field is considered to be along the thickness direction, and considering the non-zero components of strain and strain gradient, the values of stress and higher-order stress are determined as follows:

$$\begin{aligned}
\sigma_{11} &= E\left(\frac{\partial u_0}{\partial x} - z\frac{\partial \psi}{\partial x}\right) - f_1\frac{\partial P_3}{\partial z}\,,\\
\sigma_{13} &= \mu\left(-\psi + \frac{\partial w}{\partial x}\right), \qquad (19)\\
p_1 &= 2\mu l_0^2\gamma_1 + \left(f_1 + \frac{2}{3}f_2\right)P_1,\\
p_3 &= -2\mu l_0^2\frac{\partial^2\psi}{\partial x} + \left(f_1 + \frac{2}{3}f_2\right)P_3, \qquad (20)\\
\tau^{(1)}_{111} &= \frac{4\mu l_1^2}{5}\left(\frac{\partial^2 u_0}{\partial x^2} - z\frac{\partial^2\psi}{\partial x^2}\right),\\
\tau^{(1)}_{333} &= -\frac{2\mu l_1^2}{5}\left(\frac{\partial^2 w}{\partial x^2} - 2\frac{\partial\psi}{\partial x}\right),\\
\tau^{(1)}_{113} &= \tau^{(1)}_{311} = \tau^{(1)}_{131} = \frac{8\mu l_1^2}{15}\left(\frac{\partial^2 w}{\partial x^2} - 2\frac{\partial\psi}{\partial x}\right),\\
\tau^{(1)}_{223} &= \tau^{(1)}_{322} = \tau^{(1)}_{232} = -\frac{2\mu l_1^2}{15}\left(\frac{\partial^2 w}{\partial x^2} - 2\frac{\partial\psi}{\partial x}\right),\\
\tau^{(1)}_{221} &= \tau^{(1)}_{212} = \tau^{(1)}_{122} = \tau^{(1)}_{313} = \tau^{(1)}_{133} = \tau^{(1)}_{331} = -\frac{2\mu l_1^2}{5}\left(\frac{\partial^2 u_0}{\partial x^2} - z\frac{\partial^2\psi}{\partial x^2}\right), \qquad (21)
\end{aligned}$$

where E represents Young's modulus. Electric field, higher-order electric field, and electric displacement are defined as

$$\begin{aligned}
E_3 &= \alpha P_3 - f_1\frac{\partial^2 w}{\partial x^2}\,,\\
V_{33} &= \alpha\beta^2\frac{\partial P_3}{\partial z} + f_1 z\frac{\partial^2 w}{\partial x^2}\,,\\
D_3 &= -\varepsilon_0\frac{\partial\psi}{\partial z} + P_3, \qquad (22)
\end{aligned}$$

where

$$\beta^2 = \beta_1^2 + \beta_2^2 + \beta_3^2. \qquad (23)$$

By substituting the component of eq. (12) into eq. (11) and then using eqs. (8) and (10), the enthalpy variation, the kinetic energy, and the work of external forces are determined as

$$\begin{aligned}
\delta H &= \int_\forall \Big(\sigma_{ij}\delta\varepsilon_{ij} + p_i\delta\gamma_i + \tau^{(1)}_{ijk}\delta\eta^{(1)}_{ijk} + m'_{ij}\delta\chi'_{ij} + E_i\delta p_1 + V_{ij}\delta Q_{ij}\\
&\quad - \varepsilon_0\varphi_{,i}\delta\varphi_{,i} + \varphi_{,i}\delta P_i + P_i\delta\varphi_{,i}\Big)\mathrm{d}\forall + \int_\forall\left(U - \frac{1}{2}\varepsilon_0\varphi_{ij}\varphi_{ij} + \varphi_{,i}P_i\right)\delta(U_{k,k})\mathrm{d}\forall, \qquad (24)\\
\delta K &= \delta\int_0^L\left[\int\int_A\frac{1}{2}\rho\left(\left(\frac{\partial u_0}{\partial t} - z\frac{\partial\psi}{\partial t}\right)^2 + \left(\frac{\partial w}{\partial t}\right)^2\right)\mathrm{d}A\right]\mathrm{d}x\\
&= \left\{-\int_0^L\rho A\frac{\partial^2 u_0}{\partial t^2}\delta u_0\mathrm{d}x - \int_0^L\rho A\frac{\partial^2 w}{\partial t^2}\delta w\mathrm{d}x - \int_0^L\rho I\frac{\partial^2\psi}{\partial t^2}\delta\psi\mathrm{d}x\right\}, \qquad (25)\\
\delta W &= \int_0^L q(x,t)\delta w\mathrm{d}x + \left(\overline{N}\delta u_0\right)\Big|_{x=0}^{x=L} + \left(\overline{V}\delta w\right)\Big|_{x=0}^{x=L}. \qquad (26)
\end{aligned}$$

By using Hamilton's principle and applying the integration by parts and variation principle on the above equations, the general equation is obtained as

$$\int_0^T \int_0^L \left[\left(\frac{\partial N}{\partial x} - \frac{\partial^2 N^h}{\partial x^2} - \rho A \frac{\partial^2 u_0}{\partial x^2}\right)\delta u_0 + \left(\frac{\partial Q}{\partial x} - \frac{\partial^2 S}{\partial x^2} - \rho A \frac{\partial^2 w}{\partial x^2} + q\right)\delta w + \left(\frac{\partial^2 M^h}{\partial x^2} - \frac{\partial M}{\partial x} + Q - \rho I \frac{\partial^2 \psi}{\partial t^2}\right)\delta\psi\right] \mathrm{d}x\mathrm{d}t$$
$$+ \int_0^T \int_{-h/2}^{h/2} \left(E_3 - V_{33/3} + \frac{\partial \varphi}{\partial z}\right)\delta P_3 \mathrm{d}z\mathrm{d}t + \int_0^T \int_{-h/2}^{h/2} (D_{3/3})\delta\varphi \,\mathrm{d}z\mathrm{d}t - \int_0^T \left[\left(-\frac{\partial N^h}{\partial x} + N - \overline{N}\right)\delta u_0 + (N^h)\frac{\partial \delta u_0}{\partial x}\right] \mathrm{d}t\Big|_0^L$$
$$- \int_0^T \left[\left(Q - \frac{\partial s}{\partial x} - \overline{V}\right)\delta w + (S)\frac{\partial \delta w}{\mathrm{d}x}\right] \mathrm{d}t\Big|_0^L - \int_0^T \left[\left(M - \frac{\partial M^h}{\partial x}\right)\delta\psi + (M^h)\frac{\partial \delta\psi}{\partial x}\right] \mathrm{d}t\Big|_0^L$$
$$- \int_0^T \left[(V_{33})\delta P_3 + (D_3)\delta\varphi\right] \mathrm{d}t\Big|_{-h/2}^{h/2} = 0 \tag{27}$$

Finally, by taking the flexoelectric effect into consideration, the equations of motion for the Timoshenko beam can be developed as follows:

$$\begin{aligned}
&\frac{\mathrm{d}N}{\mathrm{d}x} - \frac{\mathrm{d}^2 N^h}{\mathrm{d}x^2} = \rho A \frac{\mathrm{d}^2 u_0}{\mathrm{d}t^2}\,,\\
&\frac{\partial^2 M^h}{\partial x^2} - \frac{\partial M}{\partial x} + Q = \rho I \frac{\partial^2 \psi}{\partial t^2}\,,\\
&\frac{\partial Q}{\partial x} - \frac{\partial^2 S}{\partial x^2} + q = \rho A \frac{\partial^2 w}{\partial t^2}\,, \qquad (28)\\
&E_3 - V_{33,3} + \frac{\partial \varphi}{\partial z} = 0,\\
&D_{3,3} = 0. \qquad (29)
\end{aligned}$$

Also, using eq. (27), the boundary conditions of the micro/nanobeam are determined as

$$\begin{aligned}
&N^h\Big|_0^L = 0, \quad \text{or} \quad \frac{\partial u_0}{\partial x}\Big|_0^L = 0,\\
&N - \frac{\partial N^h}{\partial x} - \overline{N}\Big|_0^L = 0, \quad \text{or} \quad u_0\Big|_0^L = 0,\\
&M - \frac{\partial M^h}{\partial x}\Big|_0^L = 0, \quad \text{or} \quad \psi\Big|_0^L = 0,\\
&M^h\Big|_0^L = 0, \quad \text{or} \quad \frac{\partial \psi}{\partial x}\Big|_0^L = 0,\\
&Q - \frac{\partial S}{\partial x} - \overline{V}\Big|_0^L = 0, \quad \text{or} \quad w\Big|_0^L = 0,\\
&S\Big|_0^L = 0, \quad \text{or} \quad \frac{\partial w}{\partial x}\Big|_0^L = 0, \qquad (30)\\
&V_{33}\Big|_{-h/2}^{h/2} = 0, \quad \text{or} \quad P_3\Big|_{-h/2}^{h/2} = 0,\\
&D_3\Big|_{-h/2}^{h/2} = 0, \quad \text{or} \quad \varphi\Big|_{-h/2}^{h/2} = 0, \qquad (31)
\end{aligned}$$

where the resultants of moment and stress as well as higher-order moment of stress are defined as

$$\begin{aligned}
N &= \int_{-h/2}^{h/2} \left(\sigma_{11} + \sigma_{11}^{Es}\right) \mathrm{d}z, \\
N^h &= \int_{h/2}^{h/2} \left(P_1 + \tau_{111}^{(1)} + m'_{23} - m'_{32}\right) \mathrm{d}z, \\
M &= \int_{-h/2}^{h/2} \left(Z\left(\sigma_{11} + \sigma_{11}^{Es}\right) + p_3 + 2\tau_{113}^{(1)} + \frac{1}{3}m'_{12} + \frac{1}{6}m'_{21}\right) \mathrm{d}z, \\
M^h &= \int_{-h/2}^{h/2} \left(p_1 + \tau_{111}^{(1)} + \frac{1}{3}m'_{23} - \frac{1}{3}m'_{32}\right) \mathrm{d}z, \\
Q &= \int_{-h/2}^{h/2} \frac{1}{2}\sigma_{13}\mathrm{d}z, \\
S &= \int_{-h/2}^{h/2} \left(\tau_{113}^{(1)} - 2m'_{21}\right) \mathrm{d}z.
\end{aligned} \tag{32}$$

Also, the electrostatic stress in eq. (32) is defined as

$$\sigma_{ki}^{ES} = \frac{1}{2}E_i P_i + \frac{1}{2}V_{ik}Q_{ij} - \frac{1}{2}\varepsilon_0 \varphi_{,i}\ \varphi_{,i} + \varphi_{,i}P_i. \tag{33}$$

5 Static analysis

5.1 Direct flexoelectric effect

In order to investigate the static deflection of the nanobeam, by substituting eqs. (22) into electric equilibrium equations (29), the following equations are obtained:

$$\begin{aligned}
\alpha P_3 - \alpha\beta^2 \frac{\partial^2 P_3}{\partial z^2} + \frac{\partial \varphi}{\partial z} &= \left(2f_1 + \frac{1}{3}f_2\right)\frac{\partial \psi}{\partial x^2} - f_2 \frac{\partial^2 w}{\partial x^2}, \\
-\varepsilon_0 \frac{\partial^2 \varphi}{\partial z^2} + \frac{\partial P_3}{\partial z^2} &= 0.
\end{aligned} \tag{34}$$

By solving the foregoing equations and considering $V_{33} = 0$ (in upper and lower beam levels) and $u_0 = 0$, polarization and electric potential are determined based on bending displacement w and cross-section rotation ψ as follows:

$$P_3 = \frac{-1}{2}\frac{\varepsilon_0 g f_1}{\alpha\varepsilon + 1} h \frac{\partial \psi}{\partial x}\frac{e^{-gh/2} + e^{gh/2}}{e^{gh} - e^{-gh}}(e^{gz} + e^{-gz}) + \frac{\varepsilon}{\alpha\varepsilon + 1}\left(-f_2\frac{\partial^2 w}{\partial x^2} + 2f_1\frac{\partial \psi}{\partial x} + \frac{1}{3}f_2\frac{\partial \psi}{\partial x}\right), \tag{35}$$

$$\varphi(z) = \frac{-1}{2}\frac{fh}{\alpha\varepsilon + 1}\frac{\partial \psi}{\partial x}\frac{e^{gh/2} + e^{-gh/2}}{e^{gh} - e^{-gh}}(e^{gz} - e^{-gz}) + \frac{1}{\alpha\varepsilon + 1}\left(-f_2(z + h/2)\frac{\partial^2 w}{\partial x^2} + f_1(2z + h/2)\frac{\partial \psi}{\partial x} + \frac{1}{3}f_2(z + h/2)\frac{\partial \psi}{\partial x}\right), \tag{36}$$

where

$$\mathrm{g} = \sqrt{\frac{1 + \alpha\varepsilon_0}{\alpha\varepsilon_0\beta^2}}. \tag{37}$$

Afterwards, using eqs. (19) to (21) and by substituting into eqs. (32), higher-order and classical moments are defined based on deflection w and cross-section rotation as

$$\begin{aligned}
M &= (T_1 - S_1)\frac{\partial \psi}{\partial x} + (S_2 - T_2)\frac{\partial^2 w}{\partial x^2}, \\
M^h &= -K\frac{\partial^2 \psi}{\partial x^2}.
\end{aligned} \tag{38}$$

Assuming A to represent beam cross-section area and I to stand for the second moment of inertia, the following relations are obtained:

$$\begin{aligned}
T_1 &= \frac{\varepsilon h}{\alpha\varepsilon+1}\left(\frac{1}{3}(f_1^2-f_1f_2)\right) - \frac{f_1^2 gh}{4(\alpha\varepsilon+1)}\frac{\left(e^{-gh/2}+e^{gh/2}\right)}{\left(e^{-gh/2}-e^{gh/2}\right)} + \frac{2f_1^2}{\alpha\varepsilon+1},\\
T_2 &= \frac{\varepsilon h}{\alpha\varepsilon+1}\left(f_1^2-f_1f_2\right),\\
S_1 &= EI + \frac{19}{10}\mu l_0^2 A + \frac{32}{15}\mu l_1^2 A + \frac{1}{2}\mu l_2^2 A,\\
S_2 &= \frac{16}{15}\mu l_1^2 A - \frac{1}{2}\mu l_2^2 A + \frac{3}{10}\mu l_0^2 A,\\
K &= \mu I\left(\frac{18}{5}l_0^2 + \frac{4}{5}l_1^2\right).\\
H_1 &= \frac{4\varepsilon h}{\alpha\varepsilon+1}(f_1f_2+f_2^2),\\
H_2 &= -\frac{4\varepsilon h}{\alpha\varepsilon+1}(f_2^2),\\
S_3 &= \frac{-6}{5}\mu l_0^2 A - \frac{16}{15}\mu l_1^2 A + 2\mu l_2^2 A,\\
S_4 &= \frac{18}{5}\mu l_0^2 A + \frac{8}{15}\mu l_1^2 A + 2\mu l_2^2 A,\\
G &= \frac{1}{2}\mu A.
\end{aligned} \tag{39}$$

By using eq. (32) and substituting eq. (38) into eq. (28), the equilibrium equations are developed as follows:

$$\begin{cases}
(T_1-S_1)\frac{\partial^2\psi}{\partial x^2} + (S_2-T_2)\frac{\partial^3 w}{\partial x^3} + k\frac{\partial^4\psi}{\partial x^4} - G\left(\frac{\partial w}{\partial x}-\psi\right) = 0,\\
G\left(\frac{\partial^2 w}{\partial x^2} - \frac{\partial\psi}{\partial x}\right) + (S_3+H_1)\frac{\partial^3\psi}{\partial x^3} + (S_4+H_2)\frac{\partial^4 w}{\partial x^4} = 0.
\end{cases} \tag{40}$$

For the cantilever beam, the boundary conditions are as follows.
At $x = 0$:

$$\begin{aligned}
\psi(0) &= 0, \qquad \psi'(0) = 0,\\
w(0) &= 0, \qquad w'(0) = 0.
\end{aligned} \tag{41}$$

At $x = L$:

$$\begin{aligned}
M - \frac{\partial M^h}{\partial x} &= 0, \qquad M^h = 0,\\
Q - \frac{\partial S}{\partial x} &= \overline{V}, \qquad Q = 0.
\end{aligned} \tag{42}$$

Finally, by using eqs. (40), the deflection equation of the cantilever beam is determined as

$$w(x) = C_1 + C_2x + C_3x^2 + C_4x^3 + C_5e^{\frac{1}{2}a_1x} + C_6e^{-\frac{1}{2}a_1x} + C_7e^{\frac{1}{2}a_2x} + C_8e^{-\frac{1}{2}a_2x}, \tag{43}$$

where the values of C_1 to C_8 as well as the values of a_1 and a_2 are determined by using boundary conditions (41) and (42).

5.2 Inverse flexoelectric effect

In the inverse flexoelectric effect, electric potential difference V is applied to the upper and lower nanobeam plane. Application of voltage causes beam deflection. The electric equilibrium equation is similar to eq. (34). With electric boundary conditions as follows,

$$\varphi\left(\frac{h}{2}\right) = V, \quad \varphi\left(-\frac{h}{2}\right) = 0 \quad \text{and} \quad V_{33} = 0, \tag{44}$$

The electric potential and polarization are extracted as follows:

$$\varphi(z)=\frac{1}{2}\frac{fh\left(\frac{\mathrm{d}^2}{\mathrm{d}x^2}w(x)\right)+V\alpha\varepsilon+V}{\alpha\varepsilon+1}+\frac{Vz}{h}-\frac{1}{2}\frac{fh\left(\frac{\mathrm{d}^2}{\mathrm{d}x^2}w(x)\right)e^{gz}}{\left(e^{-gh/2}+egh/2\right)(\alpha\varepsilon+1)}+\frac{1}{2}\frac{fh\left(\frac{\mathrm{d}^2}{\mathrm{d}x^2}w(x)\right)e^{-gz}}{\left(e^{-gh/2}+egh/2\right)(\alpha\varepsilon+1)}, \tag{45}$$

$$P_3=\frac{1}{3}\frac{1}{\alpha^2\sqrt{\alpha\varepsilon+1}}g\left(-\frac{3}{2}\frac{f_1h\left(\frac{\mathrm{d}^2}{\mathrm{d}x^2}w(x)\right)\alpha\left((\alpha\varepsilon+1)e^{zg}-(\alpha\varepsilon+1)e^{-zg}-e^{zg}+e^{-zg}\right)}{\left(e^{-\frac{1}{2}hg}+e^{\frac{1}{2}hg}\right)\sqrt{\alpha\varepsilon+1}}\right.$$
$$\left.-\frac{\sqrt{\varepsilon}\alpha^{3/2}\left(3\left(\frac{\mathrm{d}^2}{\mathrm{d}x^2}w(x)\right)hf_2-6\left(\frac{\mathrm{d}}{\mathrm{d}x}\psi(x)\right)f_1h-\left(\frac{\mathrm{d}}{\mathrm{d}x}\psi(x)\right)hf_2+3V\right)\beta}{h}\right). \tag{46}$$

By substituting the above equations into eqs. (28)–(32) the equilibrium equation and boundary conditions are determined, and the values of w and ψ are determined by solving those equations.

6 Free vibration of the Timoshenko beam

In this section, free vibration of the Timoshenko beam is investigated using the present theory and the results are obtained for a simply supported beam. Based on the equations obtained in (28), the governing equation and boundary conditions are as follows:

$$\begin{cases}(T_1-S_1)\frac{\partial^2\psi}{\partial x^2}+(S_2-T_2)\frac{\partial^3 w}{\partial x^3}+k\frac{\partial^4\psi}{\partial x^4}-G\left(\frac{\partial w}{\partial x}-\psi\right)=\rho I\frac{\partial^2\psi}{\partial t^2},\\ G\left(\frac{\partial^2 w}{\partial x^2}-\frac{\partial\psi}{\partial x}\right)+(S_3+H_1)\frac{\partial^3\psi}{\partial x^3}+(S_4+H_2)\frac{\partial^4 w}{\partial x^4}=\rho A\frac{\partial^2 w}{\partial t^2}.\end{cases} \tag{47}$$

Taking the simply supported boundary conditions into consideration yields

$$\psi'(0)=0,\qquad \psi'(L)=0,$$
$$w(0)=0,\qquad w(L)=0, \tag{48}$$
$$M-\left.\frac{\partial M^h}{\partial x}\right|_{x=0,L}=0,$$
$$\left.S\right|_{x=0,L}=0. \tag{49}$$

In order to determine the beam vibration response, first the beam response and cross-section rotation are considered as

$$w(x,t)=\sin\left(\frac{\pi x}{L}\right)e^{i\,\omega t},\qquad \psi(x,t)=\cos\left(\frac{\pi x}{L}\right)e^{i\ \omega t}, \tag{50}$$

where ω stands for beam natural frequency. By substituting the above equations in eq. (47) and using the Galerkin method, the equation of microbeam is

$$W\left(-G\left(\frac{\pi}{L}\right)^2+(S_4+H_2)\left(\frac{\pi}{L}\right)^4\right)+\psi\left(G\left(\frac{\pi}{L}\right)+(S_3+H_1)\left(\frac{\pi}{L}\right)^3\right)=-\rho Aw^2W,$$
$$W\left(-(S_2-T_2)\left(\frac{\pi}{L}\right)^3-G\left(\frac{\pi}{L}\right)\right)+\psi\left(-(T_1-S_1)\left(\frac{\pi}{L}\right)^2+K\left(\frac{\pi}{L}\right)^4+G\right)=-\rho Iw^2\psi. \tag{51}$$

By putting the above equations in order, one can write

$$\underbrace{\begin{pmatrix}X_1 & X_2\\ Y_1 & Y_2\end{pmatrix}}_{K}\begin{pmatrix}W\\ \psi\end{pmatrix}-\omega^2\underbrace{\begin{pmatrix}-\rho A & 0\\ 0 & -\rho I\end{pmatrix}}_{M}\begin{Bmatrix}W\\ \psi\end{Bmatrix}=0. \tag{52}$$

By setting the determinant of matrix of coefficients of the above equation to zero, the following equation is developed, and, by solving the following equation, the natural frequency of the nanobeam is determined:

$$\left(X_1+\rho A\omega^2\right)\left(Y_2+\rho I\omega^2\right)-X_2Y_1=0, \tag{53}$$

Table 1. Geometric specification of the beam.

$L = 100\,\text{nm}$	$h = 15\,\text{nm}$	$b = 10\,\text{nm}$

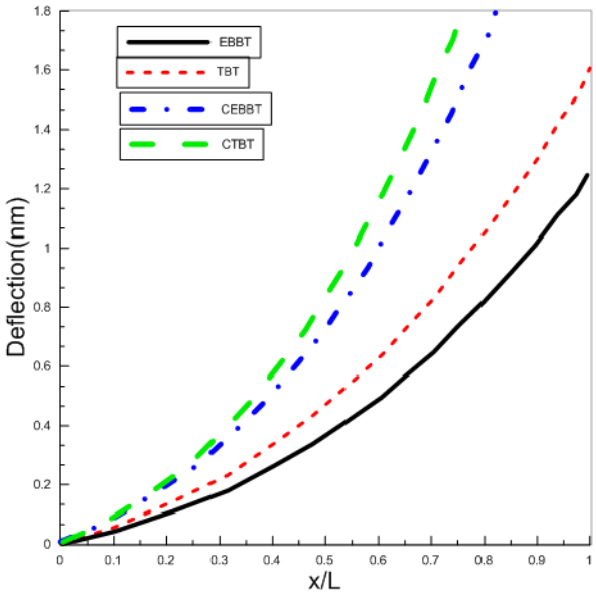

Fig. 2. Diagram of deflection of cantilever nanobeam subjected to direct flexoelectric effect.

where

$$
\begin{aligned}
X_1 &= \left(\frac{\pi}{L}\right)^2 \left(\left(\frac{\pi}{L}\right)^2 (S_4 + H) - G\right), \\
X_2 &= \left(\frac{\pi}{L}\right) \left(\left(\frac{\pi}{L}\right)^2 (T_2 - S_2) - G\right), \\
Y_1 &= \left(\frac{\pi}{L}\right) \left(\left(\frac{\pi}{L}\right)^2 (S_3 + H_1) + G\right), \\
Y_2 &= K \left(\frac{\pi}{L}\right)^4 + (S_1 - T_1) \left(\frac{\pi}{L}\right)^2 + G.
\end{aligned} \tag{54}
$$

7 Results

7.1 Static analysis

In this section, using the equations obtained in the previous section, some applicant examples are mentioned. First, deflection and electric field are determined, and, afterwards, the results yielded by the Timoshenko beam model are compared to those obtained by the Euler-Bernoulli model and the classical theory. The nanobeam is made of $BaTio_3$ and its geometric specifications are as presented in table 1.

According to ref. [10], the material properties of $BaTio_3$ are $\alpha = 0.79\text{e}8$, $\mu = 42.9\,\text{GPa}$, $\lambda = 45.2\,\text{GPa}$ and the density of the material is considered $\rho = 6020\,\text{kg/m}^3$.

In order to obtain a numerical solution, by assuming $l_0 = l_1 = l_2 = l$ and $\beta = 1$, the results are obtained for the present theory, and, by setting the size effect parameter to zero, the results are predicted based on the classical theory.

In fig. 2, the diagram of deflection of the cantilever nanobeam subjected to direct flexoelectric effect is drawn for the four models of Timoshenko beam theory (TBT), Euler-Bernoulli beam theory (EBBT), classical Timoshenko beam theory (CTBT), and classical Euler-Bernoulli beam theory (CEBBT). In this condition, the results are obtained by applying the concentrated force $F = 10\,\text{nN}$ to the beam ends and taking flexoelectric coefficients $f_1 = f_2 = 1000$ [14] into consideration. Moreover, the material properties in the Euler-Bernoulli and Timoshenko models are considered to be $l = 0.1h$ and the size effects are set to zero in the classical case.

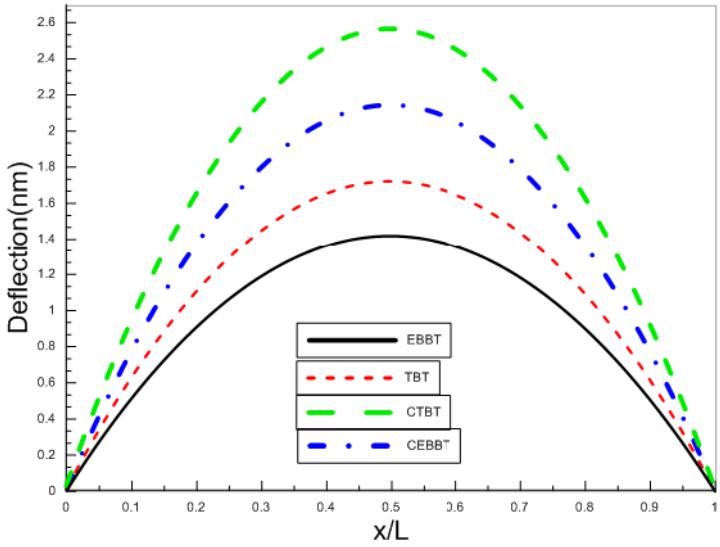

Fig. 3. Diagram of deflection of simply supported nanobeam subjected to direct flexoelectric effect.

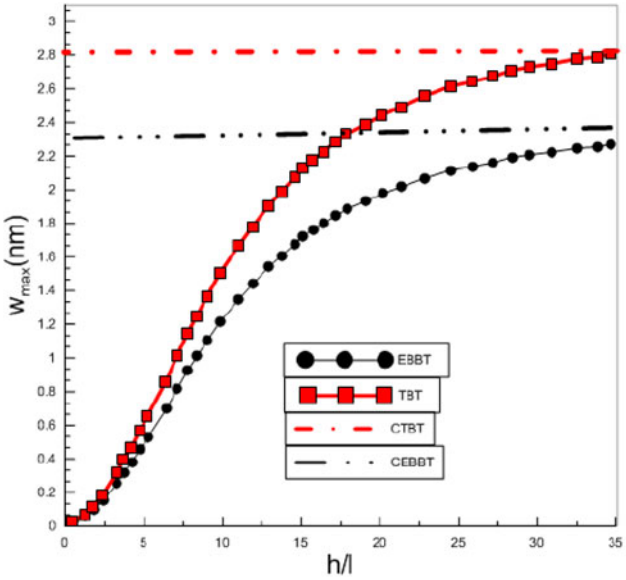

Fig. 4. Variation of maximum deflection of cantilever nanobeam in relation to the size effect parameter.

As is illustrated in fig. 2, in case of use of the present theory, the Timoshenko and Euler-Bernoulli models predict lower deflection than the classical model does, which indicates further beam stiffness in the non-classical theories in comparison to the classical ones due to the incorporation of size effects.

Figure 3 illustrates the diagram of deflection of the simply supported nanobeam subjected to direct flexoelectric effect. In this condition, the results are obtained by applying the uniform distributed force ($q_0 = 10\,\mathrm{nN/nm}$). As illustrated, in this case, too, the non-classical Timoshenko and Euler-Bernoulli models predict lower deflection than the classical model does, which indicates further beam stiffness in the non-classical theories in comparison to the classical ones due to the incorporation of size effects.

In fact, figs. 2 and 3 indicate a relationship between the mechanical behaviors of nanobeams and the type of theory (*i.e.*, classical and non-classical) under different boundary conditions.

In fig. 4, the effect of thickness-to-length scale ratio on nanobeam maximum deflection in the Euler-Bernoulli and Timoshenko models for cantilever boundary conditions is investigated. As is illustrated, as the h/l value increases, the deflection results in the Timoshenko and Euler-Bernoulli models approach toward those in the classical theory. Moreover, increasing h/l values entail an increasing difference between the results of the two Timoshenko and Euler-Bernoulli models, whereas decreasing h/l values entail a greater consistency between the two theories. Also clear from fig. 4 is that an increase in the h/l ratio is accompanied by an increase in the maximum deflection or a decrease in the beam stiffness.

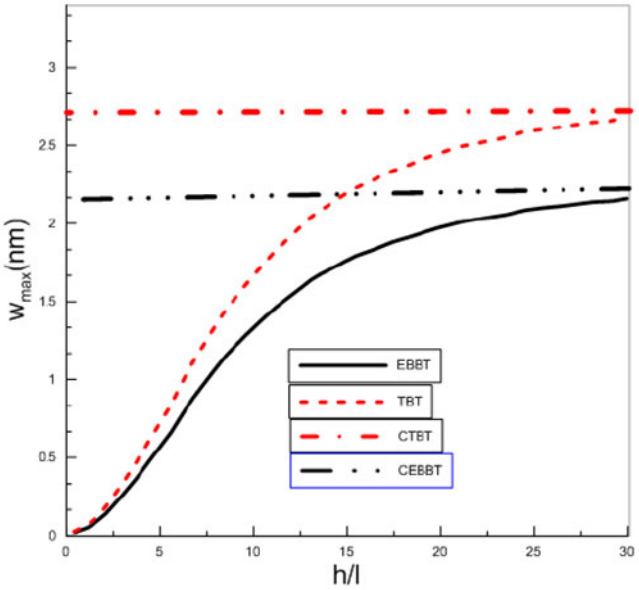

Fig. 5. Variation of maximum deflection of simply supported nanobeam in relation to the size effect parameter.

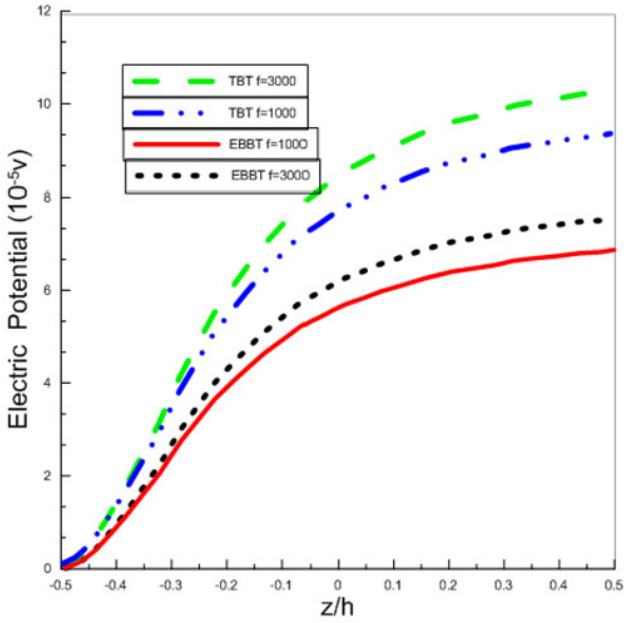

Fig. 6. Electric field distribution along beam thickness at $x = L/2$ and flexoelectric coefficient effect for cantilever beam in direct flexoelectric condition.

In fig. 5, maximum deflection is investigated in relation to the size effect parameter for simply supported boundary conditions. In this condition, too, an increase in the h/l ratio is accompanied by the widening of the gap between the results of Timoshenko and Euler-Bernoulli theories.

In fig. 6, distribution of the electric field generated along nanobeam thickness at $x = L/2$ for the cantilever beam based on Timoshenko and Euler-Bernoulli models is investigated, and the effect of flexoelectric coefficient on the results is demonstrated. As illustrated, an increase in the flexoelectric coefficient leads to an increase in the amount of the potential generated in both Timoshenko and Euler-Bernoulli models, and a decrease in the former leads to a decrease in the latter as well.

In fig. 7, distribution of the electric field generated along nanobeam thickness at $x = L/2$ for the simply supported beam based on Timoshenko and Euler-Bernoulli models is investigated. In this case, too, an increase in the flexoelectric effect is accompanied by an increase in the voltage.

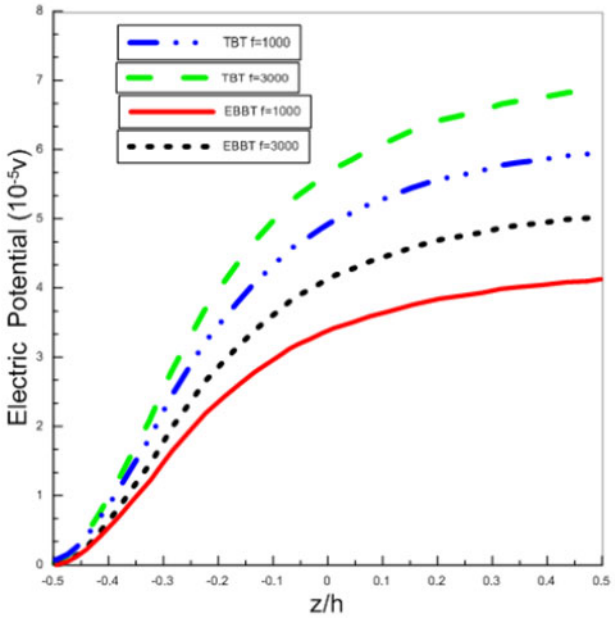

Fig. 7. Electric field distribution along beam thickness at $x = L/2$ and flexoelectric coefficient effect for simply supported beam in direct flexoelectric condition.

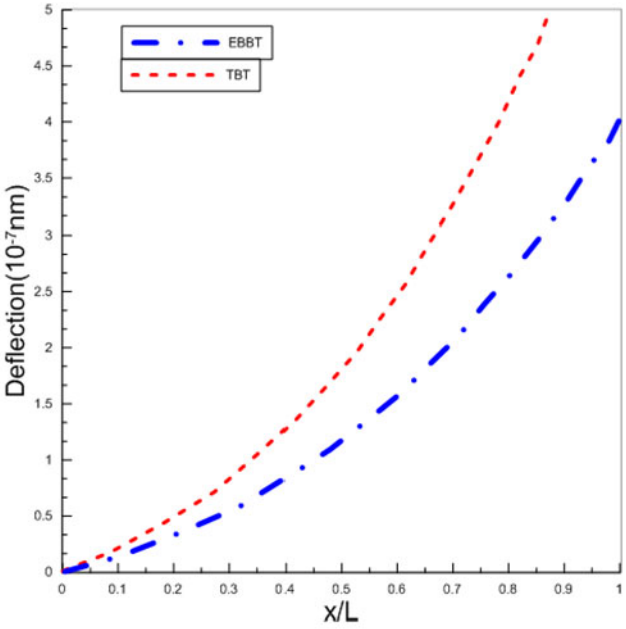

Fig. 8. Diagram of deflection of cantilever nanobeam subjected to inverse flexoelectric effect based on Euler-Bernoulli and Timoshenko theories.

Hence, it can be inferred from the above illustrations that the flexoelectricity coefficient f is crucial, since, under any circumstance, an increase in this parameter leads to an increase in the potential generated in the direct flexoelectric process. Therefore, producing a flexoelectric material with a higher flexoelectricity coefficient leads to the achievement of higher voltages. This property can be used in the design and construction of energy harvesters, because use of this flexoelectric material with a higher flexoelectric coefficient can lead to greater energy harvesting.

Figures 8 and 9 illustrate beam deflection variation under inverse flexoelectric effect at the applied voltage $V = -20v$ based on the two Timoshenko and Euler-Bernoulli models. As illustrated, firstly, regardless of the type of boundary conditions, beam deflection in the Timoshenko model is greater than that in the Euler-Bernoulli model. Secondly, the degree of deflection is dependent upon boundary conditions, and the deflection of the simply supported beam is greater than that of the cantilever beam.

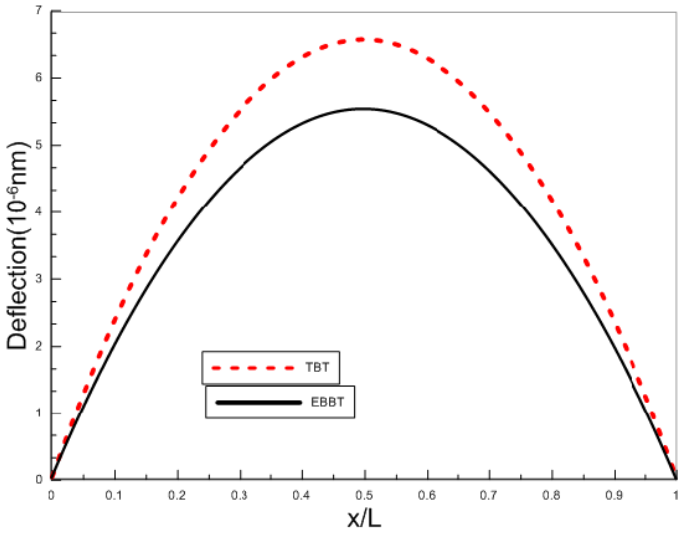

Fig. 9. Diagram of deflection of simply supported nanobeam subjected to inverse flexoelectric effect based on Euler-Bernoulli and Timoshenko theories.

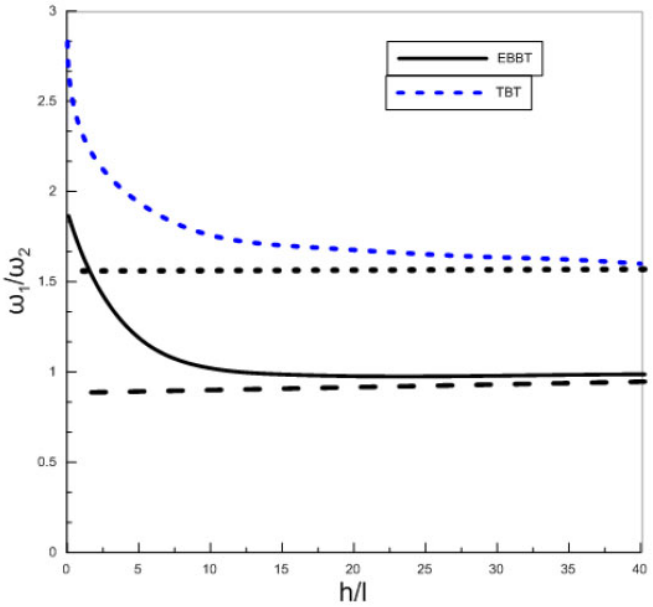

Fig. 10. Diagram of dimensionless natural frequency in relation to size effects for simply supported nanobeam based on the Euler-Bernoulli and Timoshenko theories.

7.2 Free vibration analysis

In order to demonstrate the difference in the vibration results between the Timoshenko and Euler-Bernoulli models, the dimensionless natural frequency $\omega_{1/}\omega_2$, where ω_1 represents the natural frequency of the beam in the present theory and ω_2 represents that in the classical theory, is demonstrated in relation to the size effect parameter.

Figure 10 illustrates the dimensionless frequency variation in relation to the thickness-to-length scale ratio. As illustrated, an increase in h/l value leads to a decrease in the difference between the results obtained by the present theory and those by the classical theory, while a decrease in the h/l value, *i.e.* the approaching of the size effect parameter values toward beam dimensions, such as thickness, leads to an increase in the difference between the results of the flexoelectric theory and the classical theory.

Moreover, it can be inferred from the illustration that the natural frequency predicted by the Euler-Bernoulli model is lower than that predicted by the Timoshenko model.

The last case study investigated the effect of the flexoelectric coefficient on the natural frequency of the nanobeam. Figure 11 illustrates the effect of the flexoelectric coefficient for the two Timoshenko and Euler-Bernoulli theories. As illustrated, in general, an increase in the flexoelectric effect leads to an increase in the natural frequency.

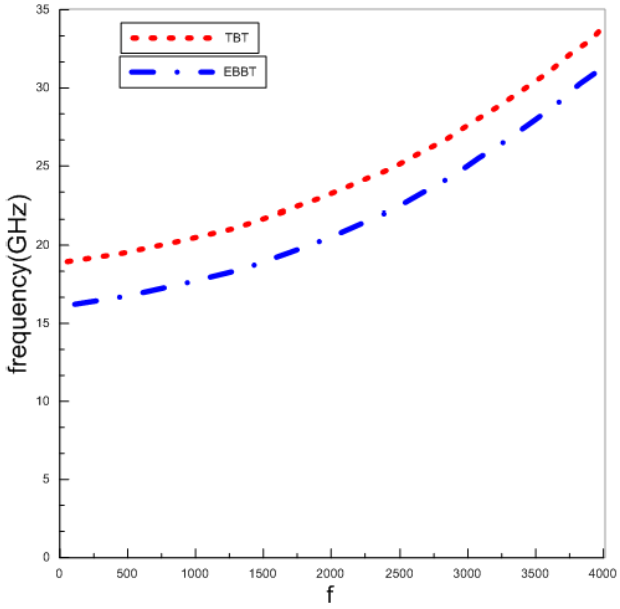

Fig. 11. Effect of flexoelectric coefficient on natural frequency of simply supported nanobeam.

Table 2. Comparison between the maximum deflection in the present study and that in ref. [10].

Maximum deflection		
	Ref. [10]	Present results
Timoshenko model	0.24244	0.2612
Euler-Bernoulli model	0.20995	0.2325

Table 3. Comparison between the voltage in the present study and that in ref. [10].

Maximum electric field		
	Ref. [10]	Present results
Timoshenko model	7.65009	7.889
Euler-Bernoulli model	7.52604	7.62

Table 4. Comparison between the natural frequency in the present study and that in ref. [10].

Natural frequency		
$L = 10h$		
	Timoshenko model	Euler-Bernoulli model
Present results	1.1245	1.195
Ref. [10]	0.98941	1.00722

7.3 Validation of the results

The results of the present study are compared with the results obtained by ref. [10], which investigated the free vibration and conducted a static analysis of the Euler-Bernoulli and Timoshenko beams subjected to surface effects. The beam used in ref. [10] is made of $BaTio_3$ with mechanical properties identical with those of the beam used in the present study.

Table 2 presents the results of maximum deflection obtained using the present theory and ref. [10]. The good consistency between the results indicates the proper formulation and solution of the present study.

Table 3 presents the results of maximum electric field, and table 4 displays natural frequency for beam thickness $h = 25\,\text{nm}$. It should be noted that the surface effects have been excluded from the comparison between the results of the present study and the results of ref. [10].

Tables 3 and 4 show good consistency between the results of the present study and the results achieved by the references for similar cases.

8 Conclusion

In this study, the size-dependent model as well as the flexoelectric formulation of Timoshenko nanobeams was developed. On the basis of the flexoelectric theory proposed by Li *et al.* and Hamilton's principle, the equations of motion and boundary conditions were investigated and the size-dependent model for a flexoelectric dielectric nanobeam was developed. The static bending and free vibration of cantilever and simply supported nanobeams were solved and some results were presented. A simply supported cantilever beam subjected to force and voltage across thickness was investigated using the Timoshenko and Euler-Bernoulli models, and the size-dependent direct and inverse flexoelectric effects were captured. The generated deflection and electric field were size-dependent, and an increase in the flexoelectric effect was accompanied by an increase in the amount of generated voltage, maximum deflection, and dimensionless natural frequencies in both Euler-Bernoulli and Timoshenko models. The results also revealed that the Timoshenko model predicts higher deflection in comparison to the Euler-Bernoulli model under identical boundary conditions. It was observed that the dimensionless natural frequencies of the dielectric nanobeams are size-dependent and increase with the increase in size parameter, and that the results of the Timoshenko beam model are higher than those of the Euler-Bernoulli model. The results are also indicative of the inappropriateness of the application of classical theories in small-scale structure frequency analysis.

References

1. Anqing Li, Shenjie Zhou, Lu Qi, Xi Chen, J. Phys. D **48**, 465502 (2015).
2. Samir A. Emam, Appl. Math. Modell. **37**, 6929 (2013).
3. Wenbin Huang, Xiang Yan, Seol Ryung Kwon, Shujun Zhang, Fuh-Gwo Yuan, Xiaoning Jiang, Appl. Phys. Lett. **101**, 252903 (2012).
4. Xiang Yan, Wenbin Huang, Seol Ryung Kwon, Shaorui Yang, Xiaoning Jiang, Fuh-Gwo Yuan, Smart Mater. Struct. **22**, 085016 (2013).
5. Yaghoub Tadi Beni, J. Intell. Mater. Syst. Struct. **27**, 2199 (2016).
6. Forough Kheibari, Yaghoub Tadi Beni, Mater. Des. **114**, 572 (2017).
7. Fahimeh Mehralian, Yaghoub Tadi Beni, Reza Ansari, Int. J. Mech. Sci. **119**, 155 (2016).
8. Fahimeh Mehralian, Yaghoub Tadi Beni, Reza Ansari, Compos. Struct. **152**, 45 (2016).
9. Sara Fattahian Dehkordi, Yaghoub Tadi Beni, Int. J. Mech. Sci. **128-129**, 125 (2017).
10. Y.M. Yue, K.Y. Xu, T. Chen, Compos. Struct. **136**, 278 (2016).
11. Z. Yan, L.Y. Jiang, J. Appl. Phys. **113**, 194102 (2013).
12. Zhi Yan, Liying Jiang, J. Phys. D: Appl. Phys. **46**, 355502 (2013).
13. ShuLing Hu, ShengPing Shen, Sci. China Phys. Mech. Astron. **53**, 1497 (2010).
14. Yaghoub Tadi Beni, Mech. Res. Commun. **75**, 67 (2016).
15. Y. Tadi Beni, J. Mech. **33**, 289 (2017).
16. Anqing Li *et al.*, Compos. Struct. **116**, 120 (2014).
17. Ali R. Hadjesfandiari, Int. J. Solids Struct. **50**, 2781 (2013).
18. Liang Xu, Shengping Shen, Int. J. Appl. Mech. **5**, 1350015 (2013).
19. Junfeng Zhao *et al.*, Appl. Math. Model. **36**, 2674 (2012).
20. H. Sadeghi, M. Baghani, R. Naghdabadi, Int. J. Eng. Sci. **50**, 22 (2012).
21. Liao-Liang Ke *et al.*, Mech. Adv. Mater. Struct. **16**, 488 (2009).
22. Wenbin Huang *et al.*, Phys. Status Solidi Rapid Res. Lett. **5**, 350 (2011).
23. M. Zamanian, S.E. Khadem, S.N. Mahmoodi, Smart Mater. Struct. **17**, 065024 (2008).
24. Shi-rong Li, Hou-de Su, Chang-jun Cheng, Appl. Math. Mech. **30**, 969 (2009).
25. Mergen H. Ghayesh, Marco Amabili, Hamed Farokhi, Int. J. Eng. Sci. **63**, 52 (2013).
26. A. Simpson, J. Mech. Eng. Sci. **15**, 159 (1973).
27. R. Davis, R.D. Henshell, G.B. Warburton, J. Sound Vib. **22**, 475 (1972).
28. D.L. Thomas, J.M. Wilson, R.R. Wilson, J. Sound Vib. **31**, 315 (1973).
29. Kanwar K. Kapur, J. Acoust. Soc. Am. **40**, 1058 (1966).
30. W.L. Cleghorn, B. Tabarrok, J. Sound Vib. **152**, 461 (1992).
31. Bo Zhang *et al.*, Finite Elements Anal. Des. **79**, 22 (2014).
32. Mesut Şimşek, Compos. Struct. **92**, 2532 (2010).
33. Aminreza Noghrehabadi *et al.*, Proc. Eng. **10**, 3750 (2011).
34. Yaghoub Tadi Beni, I. Karimipour, M. Abadyan, Appl. Math. Model. **39**, 2633 (2015).
35. Fahimeh Mehralian, Yaghoub Tadi Beni, Compos. Part B: Eng. **94**, 11 (2016).
36. H. Zeighampour, Yaghoub Tadi Beni, Acta Mech. **226**, 2607 (2015).
37. H. Zeighampour, Yaghoub Tadi Beni, Arch. Appl. Mech. **85**, 539 (2015).
38. Narges Ebrahimi, Yaghoub Tadi Beni, Steel Compos. Struct. **22**, 1301 (2016).
39. B. Akgoz, O. Civalek, Compos. Struct. **134**, 294 (2015).
40. Y.G. Wang, W.H. Lin, C.L. Zhou, Arch. Appl. Mech. **84**, 391 (2014).

41. B. Akgoz, O. Civalek, Acta Mech. **226**, 2277 (2015).
42. B. Akgoz, O. Civalek, J. Comput. Theor. Nanosci. **8**, 1821 (2011).
43. Xiao-Jun Yang *et al.*, Chaos **26**, 084312 (2016).
44. Xiao-Jun Yang, Feng Gao, H.M. Srivastava, Comput. Math. Appl. **73**, 203 (2017).
45. Xiao-Jun Yang, J.A. Tenreiro Machado, Dumitru Baleanu, Fractals **25**, 1740006 (2017).
46. R. Maranganti, N.D. Sharma, P. Sharma, Phys. Rev. B **74**, 014110 (2006).
47. Shengping Shen, Shuling Hu, J. Mech. Phys. Solids **58**, 665 (2010).
48. Z.B. Kuang, *Nonlinear Continuum Mechanics Shanghai* (Shanghai Jiaotong University Press, 2002) (in Chinese).
49. Wang, Gang-Feng, Xi-Qiao Feng., EPL **91**, 56007 (2010).